A. J.
Amrit Journal | October, 2025 | Volume 5, Issue 1 | ISSN: 2594-3235

Removal of Cr(VI) from Aqueous Solution using Bamboo Biomass Derived Hydro Char Prepared by Hydrothermal Carbonization

Purnananda Adhikari[1], Netra Prasad Subedi[1, 2], Armila Nyachhyon (Rajbhandari)[1], Sharmila Pradhan (Amatya)[3], Santosh Khanal[1]*

[1]Central Department of Chemistry, Tribhuvan University, Kirtipur Kathmandu, Nepal

[2]Central Campus of Technology, Dharan, Sunsari, Nepal

[3]Department of Chemistry, Amrit Science Campus, Kathmandu, Nepal

*Corresponding author; *santoshkhanal2003@yahoo.com*

Received: 23 June 2025; Received in revised form: 16 August 2025; Accepted: 24 August 2025

Abstract

Hydrochar is considered a promising adsorbent due to its low energy-intensive preparation along with its richness in surface functional groups. Herein, bamboo-derived hydrochar (BHC) was synthesized by hydrothermal carbonization at 200°C for four hours, and characterized by X-ray diffraction (XRD), Fourier transform infrared spectroscopy (FTIR), Scanning electron microscopy (SEM) and Brunauer-Emmett-Teller (BET) analysis. As-prepared bamboo hydrochar (BHC) was used as an adsorbent for the removal of Cr(VI) from aqueous solution. The effects of the solution pH, adsorbent dose, initial Cr(VI) concentration, and contact time were examined in a batch experiment method. The results revealed that effective Cr(VI) adsorption was facilitated by the mesoporous structure of BHC containing a large number of oxygen-containing surface functional groups. The equilibrium adsorption data supports the Langmuir isotherm and the maximum adsorption capacity for Cr(VI) is found to be 50.86 mg g^{-1} at a solution pH of 4 and an initial concentration range of 20 -150 mgL^{-1}. The equilibrium kinetic data supports a pseudo-second-order model, indicating chemisorption. BHC's potential as a sustainable adsorbent for water remediation was highlighted by the efficient Cr(VI) uptake supported by the combined mechanisms of electrostatic attraction, surface complexation, and reduction.

Keywords: *Hydrothermal carbonization; hydro char; adsorption; chromium(VI)*

1. Introduction

With the rapid industrialization and urbanization, contamination of natural water bodies with heavy metals is becoming a serious problem. Hexavalent chromium (Cr(VI)) is one of the highly toxic heavy metal, which is seen to generate from unrestrained discharge of industrial wastewater from electroplating, tanning of hides and skins, and textile manufacture (Nakkeeran, Rangabhashiyam, et al., 2016; Nakkeeran, Saranya, et al., 2016). The negative health effects associated with Cr(VI) exposure include skin irritation, respiratory problems, and

increased risk of cancer, resulting in setting a very stringent maximum permissible limit of 0.05 mg/L by the World Health Organization (Kumar & Riyazuddin, 2011; Nakkeeran et al., 2018). Therefore, creating efficient cost-effective and sustainable technologies for Cr(VI) removal has become the focus of research in environmental remediation. Among the wide range of treatments such as chemical precipitation, ion exchange, membrane filtration, and biological processes, adsorption is deemed most preferable because of its simplest operation, its low energy requirement, and its high efficacy for removal (Aigbe & Osibote, 2020; Chen et al., 2021). However, the performance of an adsorption system is determined by careful selection of an adsorbent based on relevant parameters like surface area, pore structure, and presence of functional groups able to interact with metal ions (Raji et al., 2023). Over the past few decades, researchers have investigated a wide range of materials as adsorbents for heavy metal removal, from activated carbon and zeolites to clays and more recently, bio-based materials like biochar and hydrochar (Kambo & Dutta, 2015; Velarde et al., 2023; Xie et al., 2024).

Biochar or simply char is a low-cost carbon rich materials produced from wide variety of biomass. Biochar has been used as a soil enhancer, and adsorbent for waste water treatment (Yaashikaa et al., 2020). Generally, there are two carbonization approaches for producing biochar, namely, pyrolysis and hydrothermal carbonization (HTC). In pyrolysis, dry biomass is heated in an inert atmosphere at high temperature usually from 400 to 800 ℃ depending upon the targeted applications (Ferrentino et al., 2020). However, its relevance is challenged because of highly energy- intensive preparation processes along with a decrease in the functional groups (Tomczyk et al., 2020; Wang & Wang, 2019). HTC is another approach of biochar production, which is now called hydrochar (HC). HTC is the process of heating biomass at moderate temperature (180 -250 ℃) and autogeneous pressure in an aqueous medium. One of the greatest advantages of HTC over pyrolysis is that it can deal with high moisture content biomass directly without energy-intensive drying steps (Li Yin 2016). HC typically has a moderate surface area, coupled with numerous oxygen-containing functional groups such as hydroxyl, carbonyl, and carboxyl moieties, which enhance the affinity for metal ions through electrostatic attraction, complexation, and ion exchange (Khanzada et al., 2024; Danso-Boateng et al., 2015; Peng et al., 2016).

Recent findings on the removal of chromium using HC are quite encouraging. HC prepared by Lei et al. using salix biomass has claimed to remove Cr(VI) up to 99.1% at pH 1 with superior adsorptive property compared with commercial activated carbon (Lei et al., 2018). Similarly, HC prepared from arecanut husk has been found to have decent adsorptive capacity (71.86 mg/g) of Cr(VI) (Ramesh et al., 2019). To add on, HC derived from acid-assisted poultry litter has shown strong reusability (up to four cycles without significant loss) in the removal of chromium (Ghanim et al., 2022). HC derived from Lansium domesticum peel is seen to be more efficient in higher temperatures (Siregar et al., 2022a). For the sake of feedstock, bamboo is seen as highly promising, based on its very rapid growth and endowed with the attribute of being available to most regions, for hydrochar production (Scurlock et al., 2000). Additionally, char produced from bamboo is said to have a decent surface area owing to its porosity (Han et al., 2025). Further, bamboo is asserted to be carbon dense with a huge percentage of lignocellulosic content (Sharma et al., 2019).

This study has focused on carbonization of bamboo utilizing less-energy intensive process, hydrothermal carbonization, to prepare bamboo hydro char (BHC) for effective removal of Cr(VI) from aqueous solution. As-prepared hydrochar was characterized using X-ray-diffraction (XRD), Fourier transform infrared spectroscopy (FTIR), Scanning electron microscopy (SEM) and Brunauer-Emmett-Teller (BET) to elucidate the structural and functional characteristics of BHC. The effects of various parameters for the adsorptive removal of Cr(VI) from aqueous solution was examined by batch method. Moreover, the equilibrium adsorption and kinetics data were analyzed using both linear and non-linear methods for proper description of the adsorption process.

2. Materials and Methods

2.1 Materials

Potassium dichromate ($K_2Cr_2O_7$), was obtained from sigma aldrich (India). Sulfuric acid (H_2SO_4), hydrochloric acid (HCl) sodium hydroxide (NaOH), and 1, 5-diphenylcarbazide (DPC) were obtained from Merck, India. Bamboo was procured from the local market of Kathmandu valley. All chemicals are analytical grades and used as received.

2.2 Synthesis of bamboo-derived hydrochar

The wood of the dried bamboo was washed with distilled water, crushed into fine pieces using a grinder, sieved through a 420 mesh size, and oven-dried at 105°C for 24 hr. Bamboo powder and distilled water in the mass ratio of 1:5 were added into the hydrothermal reactor, and subjected to hydrothermal carbonization at temperatures of 190 ℃, 200 ℃, and 220 ℃ for 4 hr. Hydrochar was filtered after cooling, washed repeatedly with distilled water, and finally dried in oven at 80 ℃ for 24 hr. The dried bamboo hydrochar (BHC) was crushed into finer pieces for further analysis and application.

2.3 Batch adsorption study

The adsorptive removal of Cr(VI) from an aqueous solution using BHC was carried out using batch adsorption method. Cr(VI) solution in the concentration range (20-150 mgL^{-1}) were prepared from potassium dichromate in distilled water. For the batch adsorption study, the required amount of BHC was added into an erlenmeyer flask containing 50 mL of Cr(VI) solution. The flask was shaken in mechanical shaker for 12 hr. The concentration of residual Cr(VI) after equilibrium was determined using a UV-Vis spectrometer using diphenyl carbazide method. The effect of pH was studied in the pH range (2-10) using 50 mgL^{-1} and 100 mgL^{-1} Cr(VI) solution at BHC dose of 1 gL^{-1}. The effect of BHC dose was performed in the range 0.4 – 4 gL^{-1} at pH 4. The effect of initial Cr(VI) concentration was carried out in concentration range of 20-150 mgL^{-1}, while the kinetics of adsorption was carried out at using 100 mgL^{-1} Cr(VI) solution. Both experiments were carried out at solution pH of 4.

The percentage removal and the amount of Cr(VI) adsorbed were calculated using following relations (Ghanim et al., 2022).

$$q_e = \frac{(C_o - C_e) * V}{m} \quad \text{..... (1)}$$

$$\% \, removal = \frac{(C_0 - C_e)}{C_0} * 100 \ldots\ldots\ldots\ldots\ldots\ldots\ldots\ldots (2)$$

Here, C_o and C_e represent the initial and equilibrium concentration of Cr(VI) in (mg L^{-1}) respectively, and q_e represents the adsorption capacity (mg g^{-1}). V (mL) and m (mg) represent the volume of Cr(VI) solution and mass of BHC, respectively.

2.4 Characterization

X-ray diffraction (XRD) of BHC and bamboo biomass was recorded in a Bruker D2 phase diffractometer with CuKα radiation (ƛ= 1.54 Aº) and scanning angle of 5-80º. The FTIR spectra were recorded using the Schimadzu IRA Affinity 1 instrument in the spectral range of 4000-400 cm^{-1} and a resolution of 2 cm^{-1} in AIR mode.

The morphology of the bamboo biomass and BHC was analyzed using a filed emission scanning electron microscope (FE-SEM, JEOL JSM-7610f, India) at an accelerating voltage of 5 kV. The surface of BHC and bamboo biomass was sputtered with gold prior to analysis.

Brunauer-Emmett Teller (BET) analysis was carried out using Autosorb iQ Station 1 (Quantachrome® ASiQwin™) instrument. Firstly, BHC was degassed at 150 ℃ for 3.2 hr and subjected to a vacuum to remove moisture and contaminants. The pore size distribution and total pore volume of BHC were determined by nitrogen gas adsorption and desorption at 77.35 K.

The point of Zero Charge (PZC) of BHC was determined by the pH drift method using 0.1 mol L^{-1} NaCl solution. The pH of the solution was adjusted (from 2 to 10) using 0.1 mol L^{-1} HCl and 0.1 mol L^{-1} NaOH solutions. 0.05 g of BHC was added to 25 mL NaCl solution of different pH, and the solutions were shaken with the help of a mechanical shaker at room temperature for 12 hr. The final pH of the solution was measured using the pH meter.

3. Results and discussion

3.1 Characterization of bamboo hydro char

Hydrochar from bamboo biomass was prepared by hydrothermal carbonization at three different temperature for 4 hr. The yield of BHC is found to be 70.26%, 68.25%, and 63% at 190 ℃, 200 ℃, and 220° C, respectively. The percentage yield is seen to decrease slightly on increasing hydrothermal temperature. Thus formed hydro char was subjected to methylene blue adsorption using three different concentrations of methylene blue (MB) (10, 50, 100 g/L). The concentration of MB was determined by measuring the absorbance of solution at wavelength of 664 nm, and using calibration curve. The amount of MB adsorbed is calculated using equation (1), where Ci and Ce represent the initial and equilibrium concentration of MB (in mgL^{-1}), m is the mass of BHC in mg and V is volume of solution in mL.

The amount of MB adsorbed on BHC is presented in **Figure 1.**The results showed that BHC prepared at 200°C for 4 hr have the maximum adsorptive capacity of MB at all three concentrations. The hydrochar prepared at 200°C for 4 hr. is then selected to carry out the rest of-the work.

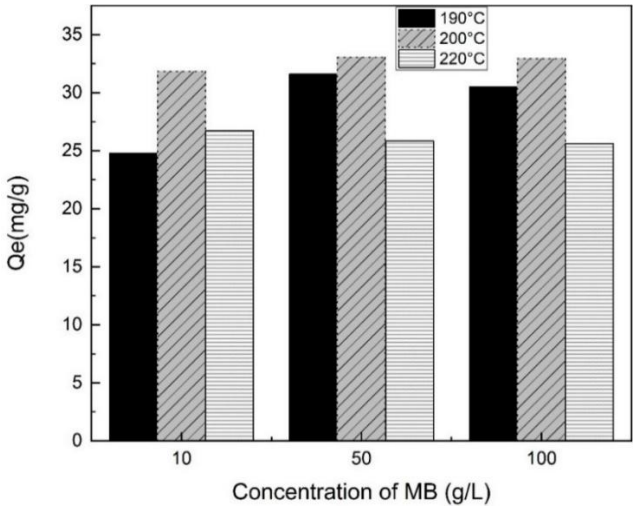

Fig. 1. Adsorption of methylene blue (MB) on BHC prepared at three different temperatures (190°C, 200°C, 220°C) for 4 h.

Figure 2(a) displays the FTIR spectra of BHC and bamboo biomass. In FTIR spectra of bamboo biomass, the broad and strong peak centered around 3387 cm^{-1} is due to the stretching of the –OH bond, and the peak around 1629 cm^{-1} is likely due to the bending of the water molecule in cellulose (Lei et al., 2018). The carbonyl group (C=O) from hemicellulose could have likely paired with the peak at 1629 cm^{-1}(D. Li et al., 2023). The peak around 2975 cm^{-1} is attributed to the methylene group bending vibration and the peak around 1360 cm^{-1} is most likely due to the aliphatic C-H stretch in cellulose and hemicellulose (Faix, 1991; Lei et al., 2018; Yu et al., 2022). Peak around 1322 cm^{-1} is likely due to the phenolic group present in cellulose (Yu et al., 2022).

Further, the peak around 1162 cm^{-1} is attributed to C-O-C asymmetric stretch vibration in cellulose and hemicellulose (Yu et al. 2022). The peak in 833 cm^{-1} is due to the presence C-H vibration in the guaiacyl derivative in lignin (Yu et al., 2024). The FTIR spectra of BHC is seen as quite similar to the biomass which shows that carbonization did not change the surface functional group of bamboo to a greater extent. However, some of the peak that are almost absent in bamboo biomass have gained more prominence with the pyrolysis. The peak is seen around 1505 cm^{-1}, which is likely due to the aromatic skeletal vibration (C=C) in lignin (Yu et al., 2024). The visible peak around 1030 cm^{-1} is due to C-O stretch in cellulose and hemicelluose and the peak around 1118 cm^{-1} is likely due to C-H groups present in lignin (Yu et al., 2022, 2024).

XRD analysis of BHC **(Figure 2(b))** shows three peaks at 15.4°, 22.4°, and 34.0° which are associated with the (101), (002), and (040) plane, respectively. These are typical of the cellulose found in the raw biomass (F. Li et al., 2020; S. Zhang et al., 2021). The similar XRD patterns of raw bamboo and BHC reinforces the idea that hydrothermal carbonization did not change the biomasses completely as discussed in FTIR analysis.

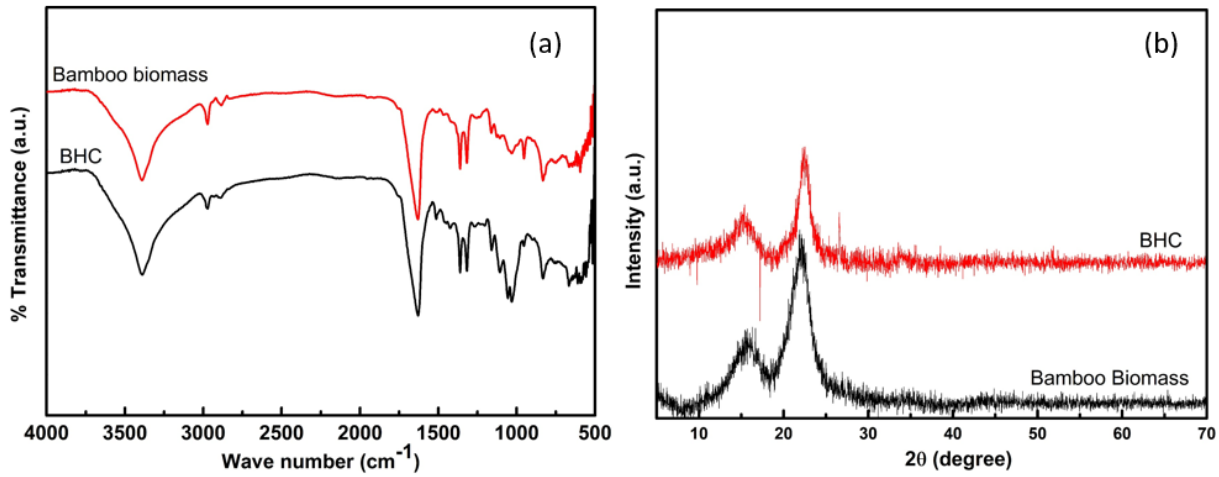

Fig. 2. a) FTIR and b) XRD of bamboo biomass and BHC.

The SEM morphology of the biomass and BHC are shown in **Figure 3.** The biomass has a flocculent or lamellar structure with a rough surface. The roughness is seen to decrease in the BHC with a bit of globular structure. Some cracks and pores could be observed in the BHC sample. **Figure 4** displays the nitrogen adsorption-desorption isotherm and pore size distribution of BHC from the BET analysis.

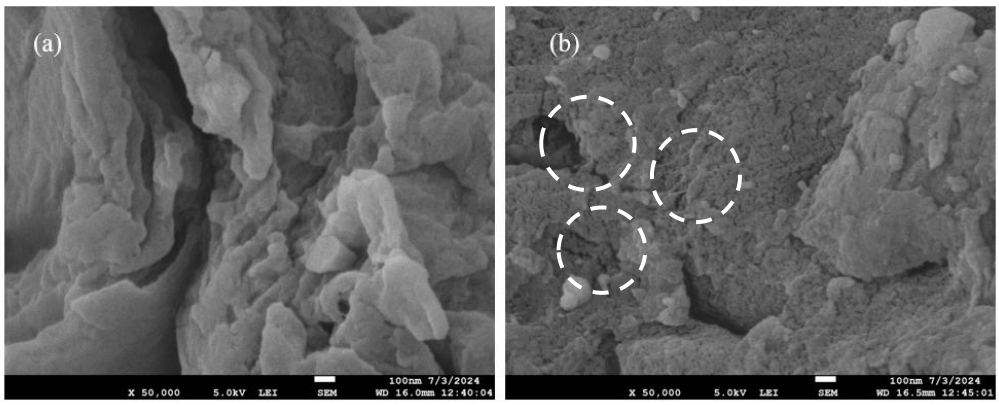

Fig. 3. SEM images of a) bamboo biomass and b) BHC.

The results indicate that BHC follows a type IV isotherm with a hysteresis loop type 3, which is attributed to the rough and non-uniform pores, i.e., micro, meso and macro-sized pores of BHC. The results of BET analysis gives the cumulative adsorption surface area of 158.9 m^2/g, the pore volume of 0.246 cm^3/g, and a pore radius of 0.905 nm using the Barrett-Joyner-Halenda (BJH) method. The total pore volume for pores with radius less than 246.8 nm at relative pressure of 0.99 is found to be 0.195 cm^3/g. Though the non-uniform pores are suggested from hysteresis loop, the type IV isotherm pattern strongly proposes the maximum mesoporous particles present in BHC (Siregar et al., 2022a; Thommes et al., 2015). So, it can be inferred that there is a wide range of pore size distribution with dominant mesopores and possibly some micropores. To add on, the H3 hysteresis (non-closing at high relative pressure)

loop is strongly suggestive of slit shaped pore characteristic in carbonaceous material (Gates et al., 2021)

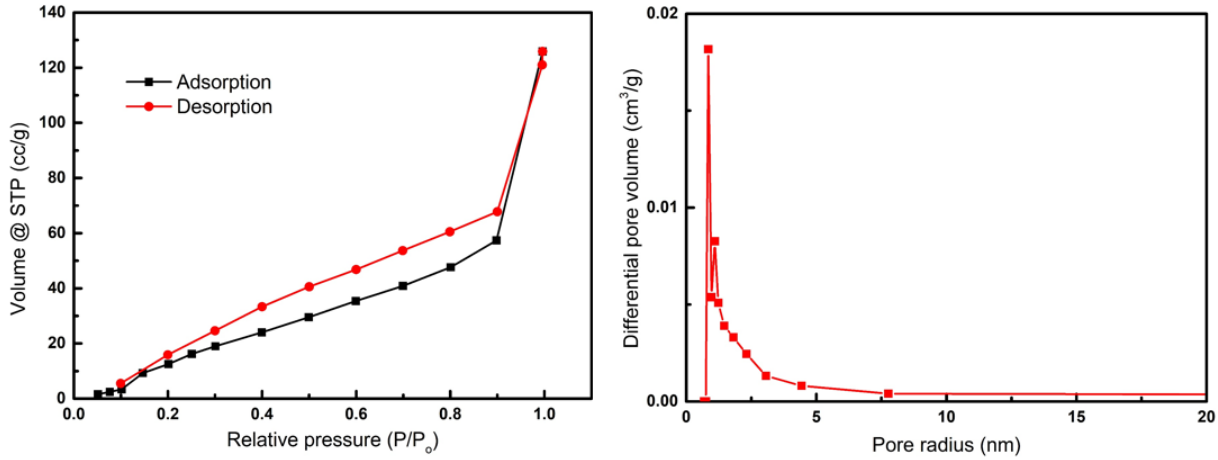

Fig. 4. a) Nitrogen adsorption and desorption isotherm, b) BJH pore size distribution for BHC.

3.2 Adsorption study

3.2.1 Effect of pH

The effect of pH on the adsorption of Cr(VI) onto BHC at different pH values ranging from 2 to 10 with the initial metal concentration of 50 mg/L and 100 mg/L is shown in **Figure 5(a)**. The maximum Cr(VI) removal using BHC is found to be 82.2% and 54.8% for Cr(VI) concentration of 50 mg/L and 100 mg/L at pH 2, respectively. Cr(VI) exist in different polyvalent species such as $Cr_2O_7^{2-}$ $HCrO_4^-$ and CrO_4^- depending upon the pH of solution. The Cr(VI) exist as $HCrO_4^-$ in aqueous solution below pH 6. At high concentration (Cr >1000 mgL^{-1}), Cr(VI) exists as $Cr_2O_7^{2-}$ in aqueous solution below pH 6 (Sengupta & Clifford, 1986). The functional groups likely gets protonated at lower pH to create a positive adsorbent surface to attract $HCrO_4^-$ resulting in high Cr(VI) removal.

Similarly, the functional groups likely gets deprotonated at higher pH to create negative adsorbent resulting in repulsion with negative chromium species decreasing the Cr(VI) removal (Ghanim et al., 2022). The point of zero charge of BHC is presented in **Figure 5(b).** The PZC of prepared BHC was found to be 7.50, which indicated that BHC surface is positively and negatively charged below and above the PZC value, respectively. As the BHC surface is positively charged at low pH, the electrostatic interaction of chromium species enhanced the adsorption. Although, pH 2 is shown to have the maximum adsorption for BHC; the rest of the adsorption experiments have been carried out at pH 4 since it is closer to the real environment.

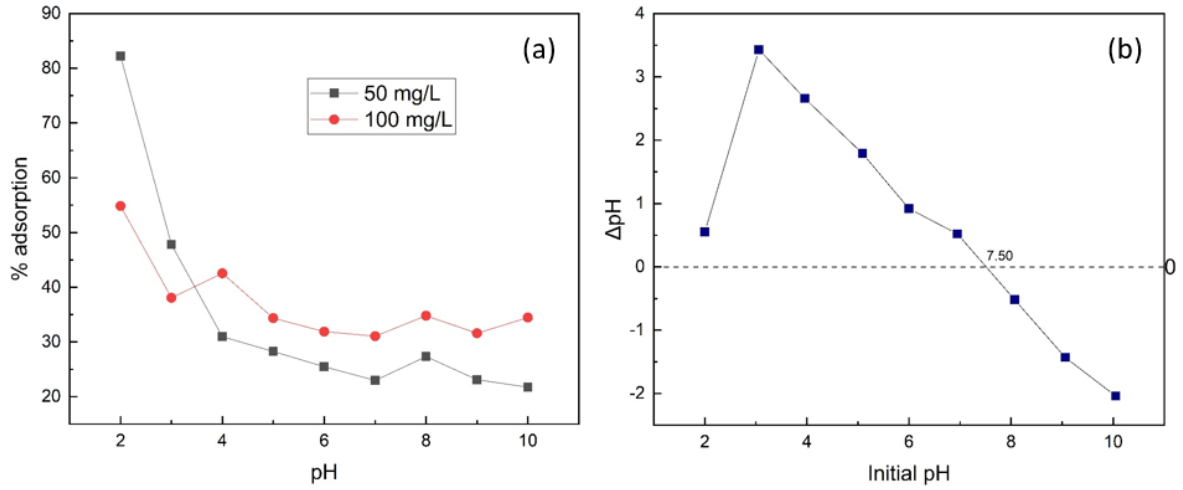

Fig. 5. a) Effect of pH on the adsorption of Cr(VI) on BHC b) pzc of BHC using 0.1M NaCl.

3.2.2 Effect of BHC dose

Figure 6 illustrates the effect of the adsorbent dose (in the range 0.5 g/L to 4.0 g/L) on the adsorption of Cr(VI) onto BHC for 50 mg/L and 100 mg/L of chromium solutions. The results indicates that the adsorption capacity of Cr(VI) decreases with the increase of the BHC dose at a fixed initial concentration of Cr(VI). At a lower dose, there is a greater chance of interaction of the BHC with Cr(VI) ion, which decreases with the increase in dose. As expected, the higher concentration (100 mg/L) has higher q_e values due to the higher accessibility of the Cr(VI) for adsorption. The high adsorption capacity, 32.3 mg/g and 110.3 mg/g by the BHC is seen in the chromium concentration of 50 mg/L and 100 mg/L, respectively at a dose of 0.5 g/L.

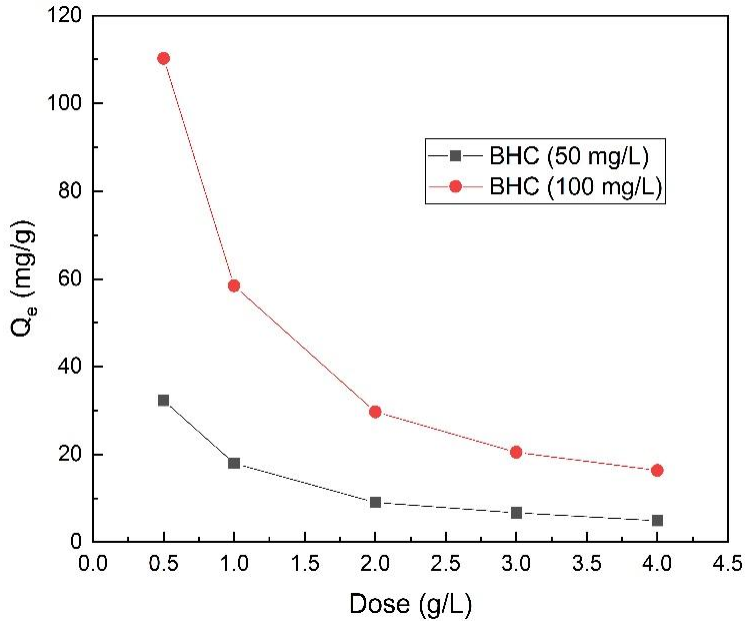

Fig. 6. Graphs showing the effect of adsorbent dose on 50 mg/L and 100 mg/ of chromium solution.

3.2.3 Isotherm model

The effect of Cr(VI) concentration on the adsorptive removal of Cr(VI) by BHC is studied in the concentration range of 20-150 mg/L. The equilibrium adsorption data were analyzed by using the Langmuir and the Freundlich adsorption isotherms. The Langmuir isotherm can be expressed in its non-linear form by equation (Ghanim et al., 2022).

$$Q_e = \frac{Q_{max} K_L C_e}{1+K_L C_e} \ldots\ldots\ldots \quad (3)$$

Where, Q_e (mg/g) represents the amount of Cr(VI) adsorbed per unit mass of BHC, K_L (L/mg) represents the Langmuir constant related to the adsorption free energy, C_e (mg/L) represents the equilibrium Cr(VI) concentration, and q_{max} (mg/g) denotes the maximum adsorption capacity for monolayer coverage (mg/g).

There are two approaches to fit the isotherm equation. In linear method, isotherm equation is transformed into a linear equation, and the isotherm parameter is then estimated from the intercept and slope of the linear curve. The coefficient of determination (R^2) is taken as the indicator for the best fit. For this purpose, the Langmuir isotherm (equation 3) is transformed into one of the linear form as:

$$\frac{C_e}{Q_e} = \frac{1}{Q_{max} K_L} + \frac{C_e}{Q_{max}} \ldots\ldots\ldots \quad (4)$$

The linear plot of Ce/Qe vs Ce is constructed based on above equation, and the resulting plot is presented in **Figure 7 (a).** The Langmuir isotherm parameters are listed in **Table 1.** The linear plot (R^2 = 0.9741) of Ce/Qe vs Ce is used to calculate maximum adsorption capacity (q_{max}) which is found to be 53.1 mg/g and the Langmuir constant (K_L) is of 0.13 Lg^{-1}.The favorability of the Langmuir isotherm process is explained by the dimensionless separation factor R_L calculated using the following relation (Ghanim et al., 2022) and values are listed in **Table 1.**

$$R_L = \frac{1}{1+K_L C_o} \ldots\ldots\ldots\ldots \quad (5)$$

Where C_o is the initial concentration of adsorbent. If R_L=1; linear, $R_L > 1$; unfavorable, in the range $0 < R_L < 1$; favorable and $R_L = 0$; irreversible (Ghanim et al., 2022). Here, it is found that the R_L values are (0.789-0.332) which are less than 1, suggesting a favorable adsorption process. Similarly, the general equation of the Freundlich isotherm is given as (Ghanim et al., 2022).

$$Q_e = K_f (C_e)^{1/n} \ldots\ldots\ldots\ldots \quad (6)$$

Equation 6 can be expressed in linear form by taking a logarithm on both sides.

$$\log Q_e = \log K_f + (1/n) \log C_e$$

Where K_f is the constant related to adsorption capacity in the Freundlich isotherm and n is the adsorption intensity (Ghanim et al., 2022). The plot of $\log Q_e$ vs $\log C_e$ gives a linear graph as shown in **Figure 7 (b).** The 1/n value calculated for BHC (0.6394) is less than 1 which shows that the adsorption process is favorable.

Table 1: Langmuir and Freundlich parameters for the adsorption of Cr(VI) into BHC from linear fit.

Langmuir isotherm model						Freundlich isotherm model			
Sample	q_{max} (mg/g)	K_L (L/mg)	R^2	SSE	R_L	K_f	1/n	R^2	SSE
BHC	53.1	0.013	0.9741	32.2	0.789-0.332	1.64	0.6394	0.9889	47.8

On the comparison, the coefficient of determination of the Langmuir isotherm (R^2=0.9741) is seen quite close to the Freundlich isotherm (R^2 = 0.9889), suggesting complex adsorption patterns; partial multilayer adsorption over non-uniform surfaces (Allen et al., 2003). However, the linear plots here are derived from non-linear equations and linearizing such inherently non-linear equation and interpreting the results with the coefficient of determination (R^2) may be coupled with errors. Hence, to get the further clarity about error, sum of squared error (SSE) analysis is performed using the relation as shown by equation (8), and values are shown in **Table 1.** The results shows that the SSE value for the Langmuir isotherm (SSE =32.2) is less than that of the Freundlich isotherm (SSE =47.8) suggesting the adsorption process is more likely to be explained by the Langmuir isotherm.

$$SSE = \sum (q_{exp} - q_{calc})^2 \ldots\ldots\ldots (8)$$

Where q_{exp} and q_{calc} are the amount of Cr(VI) adsorbed calculated experimentally and theoretically using the isotherm equations respectively.

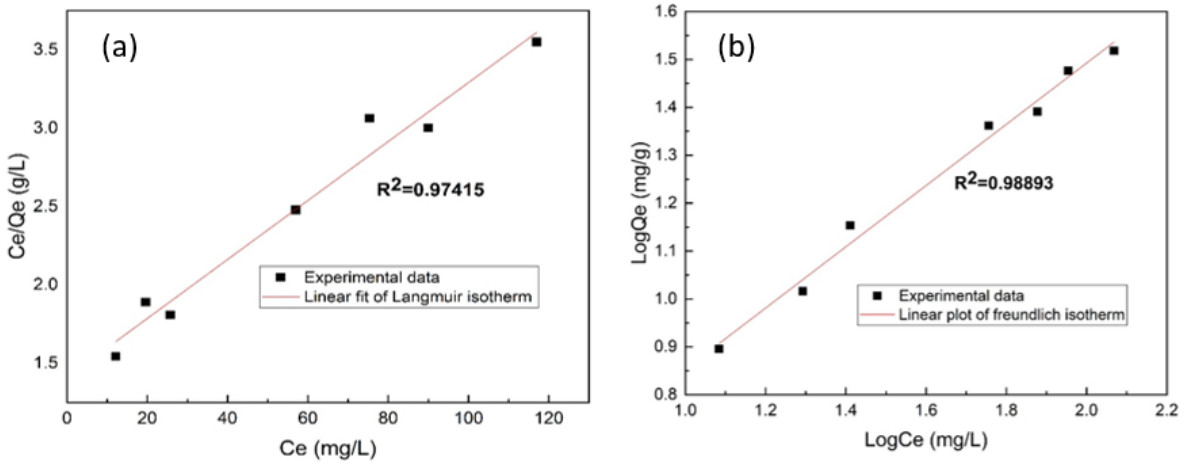

Fig. 7. a) Langmuir isotherm model b) Freundlich isotherm model (linear method).

To further optimize our adsorption process, equilibrium adsorption data is also analyzed by non-linear method using the built-in function in the Origin software as shown in **Figure 8** and isotherm parameters are collected in **Table 2**.

Table 2: Langmuir and Freundlich parameter for the adsorption of Cr(VI) into BHC from non-linear fit.

Langmuir isotherm model						Freundlich isotherm model			
Sample	q_{max} (mg/g)	K_L (L/mg)	R^2	SSE	R_L	K_f	1/n	R^2	SSE
BHC	50.86	0.015	0.9816	14.58	0.769-0.308	2.19	0.5739	0.9533	20.42

Similar to that of linear plots, the coefficient of determination (R^2) and SSE values calculated from these non-linear plots (shown in **Table 2**) show that the experimental data are best described by the Langmuir isotherm. On comparing the linear and non-linear method using SSE analysis, the non-linear plot seems more appropriate since the error values from the non-linear plot are lower compared to the linear plots. The analysis here tends to reinforce our idea that linearizing the non-linear equation is prone to errors. From these, it is inferred that the Langmuir isotherm is more appropriate to describe the Cr(VI) adsorption process onto BHC and the optimized Langmuir parameters are Q_{max} = 50.86 mg/g and K_L = 0.015 L/mg. The q_{max} value of BHC seems to be moderately good when compared to recent works for the adsorption of Cr(VI) as presented in **Table 3.**

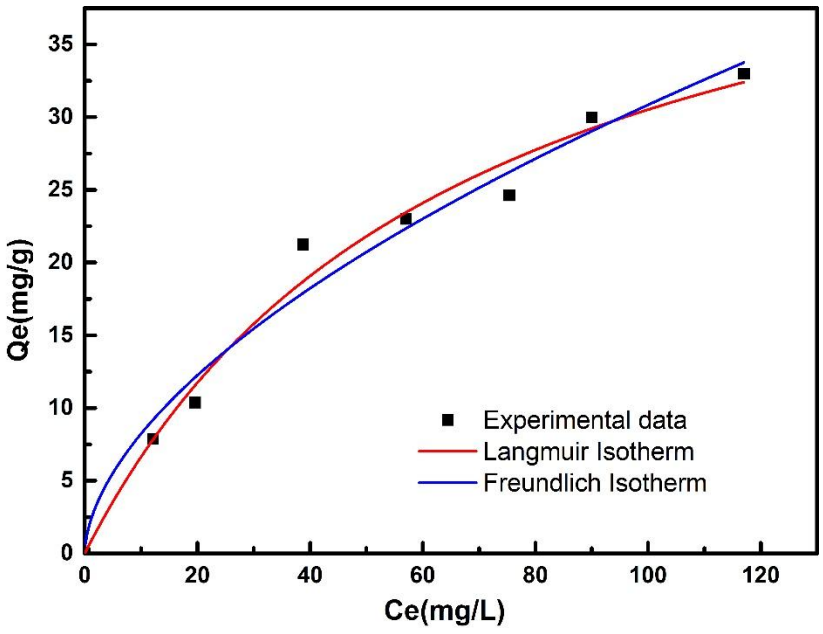

Fig. 8.: Langmuir and Freundlich isotherm (from non-linear method).

Table 3: Comparison of the maximum adsorption capacity of different adsorbents for Chromium.

Adsorbent	q_{max}(mg/g)	Reference
Poultry litter HC	26.2	(Ghanim et al., 2022)
Corn stalk biochar	26.28	(Guo et al., 2020)
Arecanut husk biomass	71.86	(Ramesh et al., 2019)
Lansium Domesticum peel HC	34.36	(Siregar et al., 2022b)
BHC	50.86	This work

Langmuir constant (K_L) is related to the free energy of adsorption given by the equation:

$$\Delta G^o = -RT\ InK \ldots\ldots\ldots \quad (9)$$

Where ΔG^o is Gibb's free energy change, T is temperature in kelvin, R is the universal gas constant, and K is the dimensionless thermodynamic equilibrium constant related to the Langmuir constant (K_L) as $K= K_L \times Mw \times 1000 \times 55.5$, where Mw is the molecular weight of the adsorbate. The value of free energy change (ΔG^o) was found to be -26.45 KJ/mol for the adsorption of Cr(IV) onto BHC. The negative value of ΔG^o shows that the adsorption process is spontaneous.

3.2.4 Kinetics study

The batch kinetic study for the adsorption of Cr(VI) onto BHC was studied by using pseudo-first-order (PFO) and pseudo-second-order (PSO) kinetic models by both non-linear regression and linear regression method. PFO model can be represented by the non-linear equation as follows (Toor & Jin, 2012):

$$q_t = q_e(1 - e^{-k_1 t}) \ldots\ldots\ldots\ldots\ldots (10)$$

Where, q_e and q_t are the uptake capacity of metal ion (mg/g) at equilibrium and at time t respectively and k_1 is the pseudo-first-order rate constant. One of the linear logarithmic equation derived from the equation (10) is given as:

$$\log(q_e - q_t) = \log(q_e) - \frac{k_1}{2.303} t \ldots\ldots\ldots\ldots\ldots (11)$$

The linear plot of log ($q_e - q_t$) vs time (t) is presented in **Figure 9 (a)**, and the obtained kinetic parameters are collected in **Table 4.** The value of K_1 (0.00361 min^{-1}) and q_e (129.02 mg/g) is evaluated for BHC from the slope and intercept. Similarly, the non-linear PSO model can be represented by the equation (Belessi et al., 2009):

$$q_t = \frac{q_e^2 k_2 t}{1+q_e^2 k_2 t} \text{ ……..(12)}$$

Where, k_2 is the pseudo-second-order rate constant.

One of the linear forms of the PSO model is given in equation (13)

$$\frac{t}{q_t} = \frac{1}{k_2 q_e^2} + \frac{1}{q_e} t \text{ .....(13)}$$

Figure 9 (b) displays the linear plot of (t/q_t) vs t, and the value of k_2 (0.000426 min^{-1}) and q_e (121.06 mg/g) is obtained from slope and intercept for BHC as shown in **Table 4.**

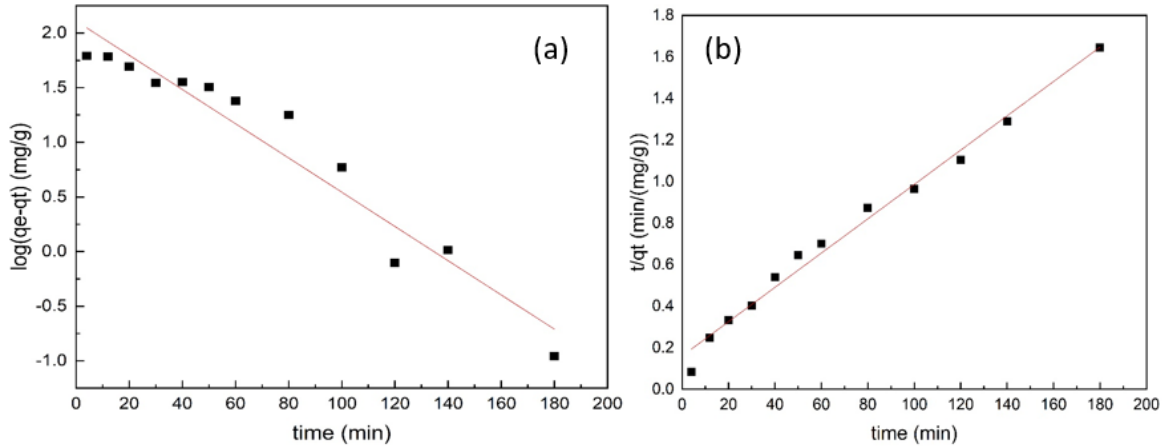

Fig. 9. a) Linear plot of the PFO model, b) Linear plot of the PSO model.

Table 4: Kinetic parameters for adsorption of Cr(VI) into BHC for 100 mg/L (linear plot)

Sample	Pseudo first order			Pseudo second order		
	q_e(mg/g)	k_1(min^{-1})	R^2	q_e(mg/g)	k_2 (g/mgmin)	R^2
BHC	129.02	0.00361	0.9351	121.06	0.000426	0.9879

Analyzing the linear plot, it can be seen that the coefficient of determination (R^2) for the PSO kinetic model (R^2 = 0.9879) is higher than that of the PFO kinetic model (Table 4). Thus, we assert that the adsorption of Cr(VI) on BHC is well described by a PSO kinetic model suggesting that chemisorption is the major rate-controlling step in the adsorption process.

The equilibrium kinetic data is also analyzed by a non-linear method for better optimization of the kinetic parameter for both the PSO and PFO model using the built-in function using Origin software. The results are displayed in **Figure 10.** The obtained kinetic parameter are collected in **Table 5.** It is found that the coefficient of determination (R^2) for PSO model is higher than that for PFO model (**Table 5)** suggesting kinetic data support the PSO model. The

optimized pseudo-second order kinetic parameter, K_2 is found to be 0.000566 g $mg^{-1}min^{-1}$, while q_e is found to be 113.85 mg/g for BHC.

Table 5: Kinetic parameters for adsorption of Cr(VI) into BHC for 100 mg/L (non-linear plot)

Sample		Pseudo first order		Pseudo second order		
	q_e(mg/g)	k_1(min^{-1})	R^2	q_e(mg/g)	k_2(g/mg min)	R^2
BHC	101.99	0.04249	0.8722	113.85	0.000566	0.9238

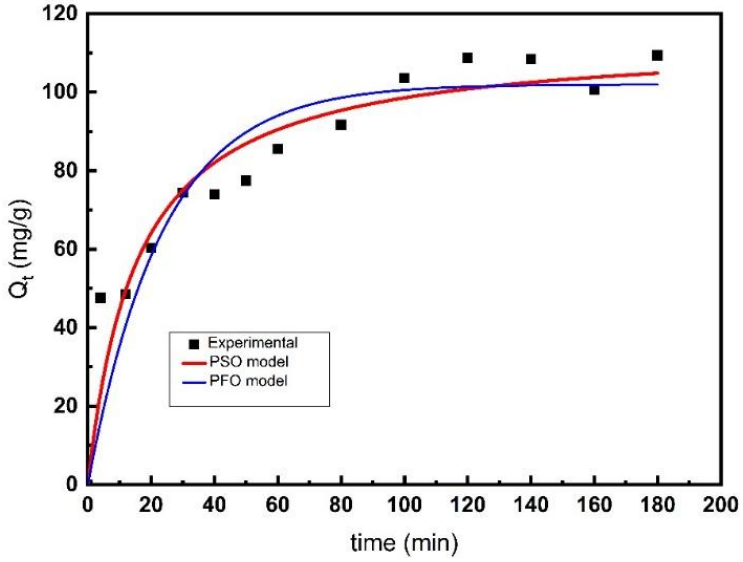

Fig. 10. Non-linear plot of PFO and PSO model.

3.3 Possible mechanism for Cr(VI) removal

The adsorption of Cr(VI) onto BHC possibly takes place through multiple routes. The functional groups (–OH, COOH) on the BHC surface likely get protonated ($-OH_2^+$), which creates the positively charged surface that attract negatively charged chromium species ($HCrO_4^-$ and $Cr_2O_7^{2-}$) via electrostatic attraction. Besides this, the electron donor group (-OH) present in BHC could reduce the part of Cr(VI) into non-toxic Cr(III). The reduced Cr(III) likely gets adsorbed via surface complexation (Vo et al., 2019; Wu et al., 2025; Y. N. Zhang et al., 2022). The schematic possible mechanism for the removal of Cr(VI) on the BHC is shown in **Figure 11.** Thus possible adsorption mechanism involves electrostatic interaction, and chemical reduction followed by surface complexation (Cheng et al., 2023).

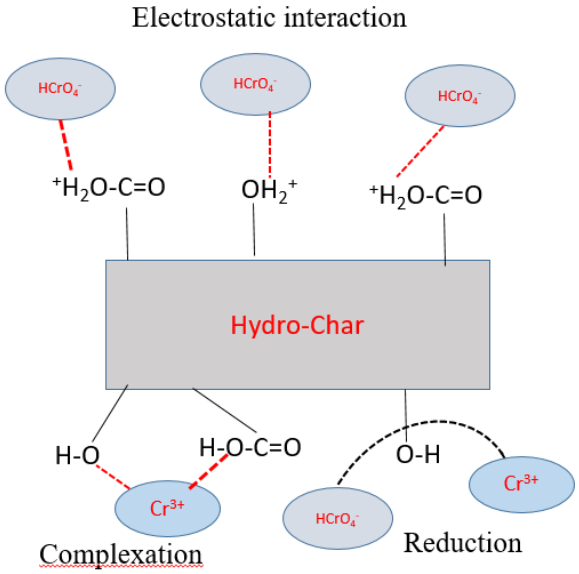

Fig. 11. Diagram showing the possible adsorption mechanisms.

4. Conclusion

In this study, bamboo-derived hydrochar (BHC) was prepared by hydrothermal carbonization of raw bamboo biomass, and utilized for the removal of Cr(VI) from aqueous solution. BET analysis showed a mesoporous nature with a pore volume of 0.246 cm^3/g, and a pore radius of 0.905 nm, while characterization techniques like FTIR and XRD demonstrated that the hydrothermal process preserved a large portion of the original biomass structure. Significant Cr(VI) removal efficiency was demonstrated by BHC in batch adsorption tests, reaching up to 82.2% removal at pH 2 while retaining good performance at pH 4, suggesting that it could potentially be a suitable material for actual wastewater conditions. The equilibrium adsorption and kinetics data are analyzed by both linear and non-linear method. The equilibrium adsorption data followed the Langmuir isotherm with a maximum monolayer adsorption capacity (q_{max}) of 50.86 mg/g from the non-linear method. The adsorption kinetic data is best described by the PSO model, suggesting chemisorption as the rate-limiting phase. Furthermore, the negative Gibbs free energy (ΔG^0 = -26.45 kJ/mol) indicated the spontaneity of adsorption process. The possible removal mechanism for Cr(VI) includes electrostatistic interaction, chemical reduction and surface complexation. Overall, the this study suggests that BHC has great potential as an inexpensive and efficient adsorbent for the remediation of Cr(VI) contaminated water because of its mesoporous structure, surface functional groups, and sustainable origin.

Acknowledgment

Authors are thankful to the University Grants Commission (UGC), Nepal for partial financial support under UGC Collaborative Research Grant number: CRG/080/081-S&T-01).

Conflict of Interest

The authors declare that there are no conflicts of interest.

References

Aigbe, U. O., & Osibote, O. A. (2020). A review of hexavalent chromium removal from aqueous solutions by sorption technique using nanomaterials. *Journal of Environmental Chemical Engineering*, *8*(6), 104503. https://doi.org/10.1016/J.JECE.2020.104503

Allen, S. J., Gan, Q., Matthews, R., & Johnson, P. A. (2003). Comparison of optimised isotherm models for basic dye adsorption by kudzu. *Bioresource Technology*, *88*(2), 143–152. https://doi.org/10.1016/S0960-8524(02)00281-X

Belessi, V., Romanos, G., Boukos, N., Lambropoulou, D., & Trapalis, C. (2009). Removal of Reactive Red 195 from aqueous solutions by adsorption on the surface of TiO 2 nanoparticles. *Journal of Hazardous Materials*, *170*(2–3), 836–844. https://doi.org/10.1016/j.jhazmat.2009.05.045

Chen, H., Zhang, Z., Zhong, X., Zhuo, Z., Tian, S., Fu, S., Chen, Y., & Liu, Y. (2021). Constructing MoS2/Lignin-derived carbon nanocomposites for highly efficient removal of Cr(VI) from aqueous environment. *Journal of Hazardous Materials*, *408*, 124847. https://doi.org/10.1016/J.JHAZMAT.2020.124847

Cheng, A., Wang, X., Liu, X., & He, C. (2023). Wet-process-modified blue-green algae biochar by K_2FeO_4 for the efficient adsorption of Cr (VI) from water. *Processes*, *11*(5), 1489.

Danso-Boateng, E., Shama, G., Wheatley, A. D., Martin, S. J., & Holdich, R. G. (2015). Hydrothermal carbonisation of sewage sludge: Effect of process conditions on product characteristics and methane production. *Bioresource Technology*, *177*, 318–327. https://doi.org/10.1016/J.BIORTECH.2014.11.096

Faix, O. (1991). Classification of Lignins from Different Botanical Origins by FT-IR Spectroscopy. *Holzforschung*, *45*(s1), 21–28. https://doi.org/10.1515/hfsg.1991.45.s1.21

Ferrentino, R., Ceccato, R., Marchetti, V., Andreottola, G., & Fiori, L. (2020). Sewage sludge hydrochar: an option for removal of methylene blue from wastewater. *Applied Sciences*, *10*(10), 3445.

Gates, W. P., Bordallo, H. N., Bouazza, A., Carnero-Guzman, G. G., Aldridge, L. P., Klapproth, A., Iles, G. N., Booth, N., Mole, R. A., Seydel, T., Yu, D., & de Souza, N. R. (2021). Neutron scattering quantification of unfrozen pore water in frozen mud. *Microporous and Mesoporous Materials*, *324*(June), 111267. https://doi.org/10.1016/j.micromeso.2021.111267

Ghanim, B., Leahy, J. J., O'Dwyer, T. F., Kwapinski, W., Pembroke, J. T., & Murnane, J. G. (2022). Removal of hexavalent chromium (Cr(VI)) from aqueous solution using acid-modified poultry litter-derived hydrochar: adsorption, regeneration and reuse. *Journal of Chemical Technology and Biotechnology*, *97*(1), 55–66. https://doi.org/10.1002/jctb.6904

Guo, X., Liu, A., Lu, J., Niu, X., Jiang, M., Ma, Y., Liu, X., & Li, M. (2020). Adsorption mechanism of hexavalent chromium on biochar: Kinetic, thermodynamic, and characterization studies. *ACS Omega*, *5*(42), 27323–27331. https://doi.org/10.1021/acsomega.0c03652

Han, S., Tao, Y., Hu, X., & Wang, G. (2025). Porous high-stiffness and damping material derived from natural bamboo: Underlying mechanisms. *Materials Today Communications*, *46*, 112911. https://doi.org/10.1016/J.MTCOMM.2025.112911

Kambo, H. S., & Dutta, A. (2015). A comparative review of biochar and hydrochar in terms of

production, physico-chemical properties and applications. *Renewable and Sustainable Energy Reviews*, *45*, 359–378. https://doi.org/10.1016/j.rser.2015.01.050

Khanzada, A. K., Al-Hazmi, H. E., Kurniawan, T. A., Majtacz, J., Piechota, G., Kumar, G., Ezzati, P., Saeb, M. R., Rabiee, N., Karimi-Maleh, H., Lima, E. C., & Mąkinia, J. (2024). Hydrochar as a bio-based adsorbent for heavy metals removal: A review of production processes, adsorption mechanisms, kinetic models, regeneration and reusability. *Science of the Total Environment*, *945*(April). https://doi.org/10.1016/j.scitotenv.2024.173972

Kumar, A. R., & Riyazuddin, P. (2011). Chromium speciation in a contaminated groundwater: Redox processes and temporal variability. *Environmental Monitoring and Assessment*, *176*(1–4), 647–662. https://doi.org/10.1007/s10661-010-1610-5

Lei, Y., Su, H., & Tian, F. (2018). A Novel Nitrogen Enriched Hydrochar Adsorbents Derived from Salix Biomass for Cr (VI) Adsorption. *Scientific Reports*, *8*(1), 1–9. https://doi.org/10.1038/s41598-018-21238-8

Li, D., Yang, S., Liu, Z., Wang, Z., Ji, N., & Liu, J. (2023). Effects of Heat Treatment under Different Pressures on the Properties of Bamboo. *Polymers*, *15*(14), 1–12.

Li, F., Zimmerman, A. R., Hu, X., & Gao, B. (2020). Removal of aqueous Cr(VI) by Zn- and Al-modified hydrochar. *Chemosphere*, *260*. https://doi.org/10.1016/j.chemosphere.2020.127610

Nakkeeran, E., Patra, C., Shahnaz, T., Rangabhashiyam, S., & Selvaraju, N. (2018). Continuous biosorption assessment for the removal of hexavalent chromium from aqueous solutions using Strychnos nux vomica fruit shell. *Bioresource Technology Reports*, *3*(August), 256–260. https://doi.org/10.1016/j.biteb.2018.09.001

Nakkeeran, E., Rangabhashiyam, S., Giri Nandagopal, M. S., & Selvaraju, N. (2016). Removal of Cr(VI) from aqueous solution using Strychnos nux-vomica shell as an adsorbent. *Desalination and Water Treatment*, *57*(50), 23951–23964. https://doi.org/10.1080/19443994.2015.1137497

Nakkeeran, E., Saranya, N., Giri Nandagopal, M. S., Santhiagu, A., & Selvaraju, N. (2016). Hexavalent chromium removal from aqueous solutions by a novel powder prepared from Colocasia esculenta leaves. *International Journal of Phytoremediation*, *18*(8), 812–821. https://doi.org/10.1080/15226514.2016.1146229

Peng, C., Zhai, Y., Zhu, Y., Xu, B., Wang, T., Li, C., & Zeng, G. (2016). Production of char from sewage sludge employing hydrothermal carbonization: Char properties, combustion behavior and thermal characteristics. *Fuel*, *176*, 110–118. https://doi.org/10.1016/J.FUEL.2016.02.068

Raji, Z., Karim, A., Karam, A., & Khalloufi, S. (2023). Adsorption of Heavy Metals: Mechanisms, Kinetics, and Applications of Various Adsorbents in Wastewater Remediation—A Review. *Waste*, *1*(3), 775–805. https://doi.org/10.3390/waste1030046

Ramesh, S., Sundararaju, P., Banu, K. S. P., Karthikeyan, S., Doraiswamy, U., & Soundarapandian, K. (2019). Hydrothermal carbonization of arecanut husk biomass: fuel properties and sorption of metals. *Environmental Science and Pollution Research*, *26*(4), 3751–3761. https://doi.org/10.1007/s11356-018-3888-8

Scurlock, J. M. O., Dayton, D. C., & Hames, B. (2000). Bamboo: an overlooked biomass resource? *Biomass and Bioenergy*, *19*(4), 229–244. https://doi.org/10.1016/S0961-9534(00)00038-6

Sengupta, A. K., & Clifford, D. (1986). Chromateion Exchange Mechanism for Cooling Water. *Industrial and Engineering Chemistry Fundamentals*, *25*(2), 249–258. https://doi.org/10.1021/i100022a012

Sharma, H. B., Panigrahi, S., & Dubey, B. K. (2019). Hydrothermal carbonization of yard waste for solid bio-fuel production: Study on combustion kinetic, energy properties, grindability and flowability of hydrochar. *Waste Management*, *91*, 108–119. https://doi.org/10.1016/j.wasman.2019.04.056

Siregar, P. M. S. B. N., Wijaya, A., Amri, Nduru, J. P., Hidayati, N., Lesbani, A., & Mohadi, R. (2022a). Layered Double Hydroxide/C (C=Humic Acid;Hydrochar) As Adsorbents of Cr(VI). *Science and Technology Indonesia*, *7*(1), 41–48. https://doi.org/10.26554/sti.2022.7.1.41-48

Siregar, P. M. S. B. N., Wijaya, A., Amri, Nduru, J. P., Hidayati, N., Lesbani, A., & Mohadi, R. (2022b). Layered Double Hydroxide/C (C=Humic Acid;Hydrochar) As Adsorbents of Cr(VI). *Science and Technology Indonesia*, *7*(1), 41–48. https://doi.org/10.26554/STI.2022.7.1.41-48

Thommes, M., Kaneko, K., Neimark, A. V., Olivier, J. P., Rodriguez-Reinoso, F., Rouquerol, J., & Sing, K. S. W. (2015). Physisorption of gases, with special reference to the evaluation of surface area and pore size distribution (IUPAC Technical Report). *Pure and Applied Chemistry*, *87*(9–10), 1051–1069. https://doi.org/10.1515/pac-2014-1117

Tomczyk, A., Sokołowska, Z., & Boguta, P. (2020). Biochar physicochemical properties: pyrolysis temperature and feedstock kind effects. *Reviews in Environmental Science and Biotechnology*, *19*(1), 191–215. https://doi.org/10.1007/S11157-020-09523-3/TABLES/3

Toor, M., & Jin, B. (2012). Adsorption characteristics , isotherm , kinetics , and diffusion of modified natural bentonite for removing diazo dye. *Chemical Engineering Journal*, *187*, 79–88. https://doi.org/10.1016/j.cej.2012.01.089

Velarde, L., Nabavi, M. S., Escalera, E., Antti, M. L., & Akhtar, F. (2023). Adsorption of heavy metals on natural zeolites: A review. *Chemosphere*, *328*(February), 138508. https://doi.org/10.1016/j.chemosphere.2023.138508

Vo, A. T., Nguyen, V. P., Ouakouak, A., & Nieva, A. (2019). water E ffi cient Removal of Cr (VI) from Water by Biochar and Activated Carbon Prepared through Hydrothermal Carbonization and Pyrolysis : *Mdpi*, *11*(Vi), 1–14.

Wang, J., & Wang, S. (2019). Preparation, modification and environmental application of biochar: A review. *Journal of Cleaner Production*, *227*, 1002–1022. https://doi.org/10.1016/J.JCLEPRO.2019.04.282

Wu, M., Ouyang, X., Li, Y., Zhang, J., Liu, J., & Yin, H. (2025). Mechanisms in Hexavalent Chromium Removal from Aquatic Environment by the Modified Hydrochar-Loaded Bacterium Priestia megaterium Strain BM.1. *Sustainability (Switzerland)*, *17*(11), 1–19. https://doi.org/10.3390/su17115172

Xie, S., Huang, L., Su, C., Yan, J., Chen, Z., Li, M., Du, M., & Zhang, H. (2024). Application of clay minerals as adsorbents for removing heavy metals from the environment. *Green and Smart Mining Engineering*, *1*(3), 249–261. https://doi.org/10.1016/j.gsme.2024.07.002

Yaashikaa, P. R., Kumar, P. S., Varjani, S., & Saravanan, A. (2020). A critical review on the biochar production techniques, characterization, stability and applications for circular

bioeconomy. *Biotechnology Reports*, *28*, e00570. https://doi.org/10.1016/J.BTRE.2020.E00570

Yu, H., Gui, C., Ji, Y., Li, X., Rao, F., Huan, W., & Li, L. (2022). Changes in Chemical and Thermal Properties of Bamboo after Delignification Treatment. *Polymers*, *14*(13), 1–11. https://doi.org/10.3390/polym14132573

Yu, H., Zhang, Y., Li, J., & Rao, F. (2024). Structural characteristics and physicomechanical properties of bamboo scrimber composite during natural weathering. *Surfaces and Interfaces*, *51*(July), 104714. https://doi.org/10.1016/j.surfin.2024.104714

Zhang, S., Sheng, K., Yan, W., Liu, J., Shuang, E., Yang, M., & Zhang, X. (2021). Bamboo derived hydrochar microspheres fabricated by acid-assisted hydrothermal carbonization. *Chemosphere*, *263*, 128093. https://doi.org/10.1016/J.CHEMOSPHERE.2020.128093

Zhang, Y. N., Guo, J. Z., Wu, C., Huan, W. W., Chen, L., & Li, B. (2022). Enhanced removal of Cr(VI) by cation functionalized bamboo hydrochar. *Bioresource Technology*, *347*(December 2021), 126703. https://doi.org/10.1016/j.biortech.2022.126703